Available online at www.sciencedirect.com
SCIENCE DIRECT
Polymer 46 (2005) 9404–9410
polymer
www.elsevier.com/locate/polymer

Structure formation in poly(ethylene terephthalate) upon annealing as revealed by microindentation hardness and X-ray scattering

A. Flores[a], M. Pieruccini[b], N. Stribeck[c], S.S. Funari[d], E. Bosch[a], F.J. Baltá-Calleja[a,*]

[a]*Instituto de Estructura de la Materia, CSIC, Serrano 119, 28006 Madrid, Spain*
[b]*CNR, Istituto per i Processi Chimico-Fisici Sez. Messina, Via La Farina 237, I-98123 Messina, Italy*
[c]*Institut für Technische und Makromolekulare Chemie der Universität Hamburg, Hamburg, Germany*
[d]*Hasylab, DESY, Notkestrasse 85, D-22607 Hamburg, Germany*

Received 8 March 2005; received in revised form 7 July 2005; accepted 11 July 2005
Available online 10 August 2005

Abstract

The micromechanical properties (microindentation hardness, H, elastic modulus, E) of poly(ethylene terephthalate) (PET), isothermally crystallized at various temperatures (T_a) from the glassy state are determined to establish correlations with thermal properties and nanostructure. Analysis of melting temperature and crystal thickness derived from the interface distribution function analysis of SAXS data reveals that for $T_a < 190$ °C the occurrence of two lamellar stack populations prevails whereas for samples annealed at $T_a > 190$ °C a population of lamellar stacks with a unimodal thickness distribution emerges. The H and E-values exhibit a tendency to increase with the degree of crystallinity. The results support a correlation $E/H \sim 20$ in accordance with other previously reported data. The changes of microhardness with annealing temperature are discussed in terms of the crystallinity and crystalline lamellar thickness variation. Unusually high hardness values obtained for PET samples crystallized at $T_a = 190$ °C are discussed in terms of the role of the rigid amorphous phase which offers for the hardness of amorphous layers constrained between lamellar stacks a value of $H_a \sim 150$ MPa. On the other hand, for $T_a =$ 240 °C the decreasing H-tendency could be connected with the chemical degradation of the material at high temperature.

Keywords: Polyethylene terephthalate; Microhardness; Elastic modulus

1. Introduction

Microindentation hardness is a convenient tool for the investigation of the mechanical properties of polymers. Being a simple and rapid technique, it has been widely proved to be extremely sensitive to nanostructural changes taking place in a polymer material [1–4]. Variations in the degree of crystallinity, the lamellar thickness, or the surface free energy of the crystals can be readily detected by means of microindentation hardness [1,5–7]. On the other hand, for homogenous polymer materials, microhardness, H, is directly correlated to the yield stress [8,9].

Microindentation hardness has been employed in a number of preceding studies for the investigation of the mechanical behaviour of poly(ethylene terephthalate) (PET), aiming at establishing correlations between the diverse nanostructures emerging upon crystallization and the corresponding micromechanical properties [10,11]. It is now well established that during primary crystallization the microhardness of PET is mainly dependent on the volume degree of crystallizing units (spherulites) [10]. On the other hand, for fully crystallized PET, microhardness depends linearly on the degree of crystallinity, and is also a function of the specific morphology of the crystal lamellae, such as the crystal thickness and the surface free energy of the crystals [10–12].

The semicrystalline nanostructure of PET, whether it is constituted by lamellae stacks separated by pockets of amorphous material, or by homogeneously distributed lamellar stacks, is still a matter of debate [13,14]. It has also been suggested that, in addition to the mobile amorphous and the crystalline regions, a third phase, the rigid amorphous fraction (RAF), is present in semicrystalline PET [15–17]. The nature of the RAF could be

* Corresponding author.
E-mail address: embalta@iem.cfmac.csic.es (F.J. Baltá-Calleja).

0032-3861/$ - see front matter © 2005 Elsevier Ltd. All rights reserved.
doi:10.1016/j.polymer.2005.07.033

envisaged in the two following ways: (i) Arising from the thin amorphous layers constrained between the crystalline lamella; the lamellae stacks are separated by thicker amorphous layers (mobile amorphous fraction) [16], or (ii) occurring at the crystal–amorphous interface in the basal lamellar planes; the rigid amorphous phase gradually merges into the mobile one when approaching the amorphous bulk [17].

Recent microindentation measurements carried out in glassy oriented PET, crystallized at various T_a, suggest that the hardness of the amorphous interfibrilar regions within the crystallized material is higher than that of the amorphous starting one [18]. Hence, it seems that the formation of rigid amorphous regions inherent to crystallization produces a concomitant variation of the mechanical properties that can be detected by means of microindentation hardness.

The present paper aims to complement the foregoing investigations offering a study of the micromechanical behaviour of a series of isotropic PET samples, cold crystallized at various temperatures, in relation to their nanostructure. The study explores the need of accounting for a rigid amorphous fraction to explain the mechanical behaviour of the annealed materials.

2. Experimental

2.1. Materials

The starting glassy PET material (Goodfellow, ES301465, $M_w = 20{,}000$ g/mol) was supplied in the form of films ≈ 350 μm thick. Rectangular-shaped samples were cut from the as-received sheets and crystallized for 9 h at different annealing temperatures in the range 120–240 °C. The crystallization process was carried out in nitrogen to limit oxidative degradation.

2.2. Techniques

Differential calorimetry measurements were carried out using a Perkin–Elmer DSC-7 in the range from 50 to 300 °C, using a heating rate of 10 °C/min under a nitrogen flux. The heat of fusion is derived from the area under the melting peak. Calibration of the temperature and of the heat of fusion was made using indium. The degree of crystallinity, α_{DSC}, is calculated from the ratio of the sample heat of fusion to the enthalpy of fusion of a completely crystalline sample ($\Delta h_f^0 = 135$ J/g) [10,11]. Some of the annealed PET samples exhibit two melting endotherms during the heating cycle (Table 1). The melting endotherm at high temperatures seems to be associated to primary crystallization, while that at low temperatures appears to be due to the melting of secondary lamellae [19]. Hence, both melting endotherms have been taken into account in the calculation of α_{DSC}.

Wide angle X-ray diffraction (WAXS) patterns were obtained using a Seifert goniometer operating in a theta–theta configuration, attached to a Seifert generator operating at 40 kV and 35 mA. The divergence slits used were of 2 and 1°. The antiscattering slits employed were of 0.3 and 0.2°. The WAXS patterns were recorded in the range $5° \leq 2\theta \leq 90°$, at steps of 0.01°, using an accumulation time of 10 s. A silicon standard was used for calibration purposes. The amorphous halo of glassy PET was fitted to the diffraction curve of each annealed sample for the estimation of the degree of crystallinity, α_{WAXS}, which was determined from the ratio of the area under the crystalline peaks to that of the total diffraction curve.

Small angle X-ray diffraction measurements were obtained using a synchrotron radiation source at DESY, HASYLAB (beamline A2). Scattering patterns were recorded using a one-dimensional detector. The data were corrected for the detector response and beam intensity, and calibrated against a rat tendon tail standard. A wavelength of 1.50 Å was employed. The average values of the thicknesses of the amorphous and crystalline layers were determined from the interface distribution function (IDF), following a procedure analogous to the one described in Ref. [20]. The IDF function of each sample was fitted to Gaussian type distributions, assuming a statistical model of flat extended lamellar stacks. It has been assumed that the crystalline component exhibits narrower thickness distributions than the amorphous one.

Microhardness measurements were carried out at room temperature (23 °C) using a Vickers diamond attached to a Leitz tester. The indenter penetrates the sample surface at a given load, P, for 6 s. The diagonal of the residual impression, d, left behind upon load release, is measured using an optical microscope. Microhardness values, H, are derived from the linear regression of P versus d^2, following [1]:

$$H = \frac{1.85P}{d^2} \tag{1}$$

Loads of 0.49, 0.98 and 1.96 N were employed. Additionally, a load of 2.94 N was used for the samples annealed at 220 and 240 °C.

Elastic modulus values were determined by means of a Shimadzu ultra-microhardness depth-sensing instrument. A Vickers pyramid indenter was also used in this case. Continuous load-displacement monitoring as the indenter is driven and withdrawn from the film substitutes the imaging method described above. The load is increased at constant rate (4.41 mN/s) up to the peak load (147 mN), held thereafter for 200 s and subsequently reduced at the same rate as in the loading cycle. These experimental conditions are selected to promote an elastic response of the material at the beginning of the unloading cycle, necessary for the determination of the elastic modulus values [9]. On the one hand, large hold times at peak load (200 s) minimize creep effects during the initial stages of unloading; on the other, the unloading rate employed (4.41 mN/s) yields an unloading strain rate at the beginning of the unloading 10

Table 1
Degree of crystallinity values derived from WAXS and DSC, α_{WAXS} and α_{DSC}, respectively, melting points, T_m, obtained from DSC (heating rate: 10 °C/min), microhardness, H, elastic modulus, E, E/H ratio, crystal thickness, l_c and linear degree of crystallinity, α_L for the various PET samples annealed at various temperatures

T_a (°C)	T_{m1} (°C)	T_{m2} (°C)	α_{DSC}	α_{WAXS}	H (MPa)	E (GPa)	E/H	l_c (nm)	α_L
25			0	0	127±1	3.16±0.08	25		
120	142.8	243.9	0.26	0.30	176±2	3.49±0.08	20	2.7	0.39
140	157.8	244.0	0.26	0.30	182±1	3.57±0.07	20	2.8	0.42
160	182.0	244.1	0.29	0.32	188±1	3.60±0.09	19	3.3	0.47
190	217.1	247.4	0.35	0.35	219±3	4.00±0.07	18	3.3	0.41
220	241.3		0.40	0.35	216±2	3.93±0.08	18	4.2	0.42
240	263.8		0.41	0.44	211±2	4.2±0.1	20	6.2	0.47

times greater than that at the end of the hold time. Elastic modulus values, E, can be determined from the analysis of the load-unloading curves, following [21]:

$$E_r = \sqrt{\frac{\pi}{24.5 h_c^2}}\frac{S}{2} \quad (2)$$

where

$$\frac{1}{E_r} = \frac{1-\nu^2}{E} + \frac{1-\nu_0^2}{E_0}$$

and where $S=(\partial P/\partial h)_{max}$ is the initial unloading stiffness during unloading, h_c is the contact penetration depth at peak load, E_r the reduced modulus, E and ν Young's modulus and Poisson's ratio of the material, respectively, and E_0 and ν_0 Young's modulus and Poisson's ratio of the diamond indenter, respectively. In our case, the $(1-\nu_0^2)/E_0$ term can be neglected. Poisson's ratio for PET is taken to be 0.30 for the glassy material and 0.35 for the semicrystalline one [22]. $(\partial P/\partial h)_{max}$ is determined by analytically differentiating a power law function fitted to the upper one fourth of the unloading curve and calculating the derivative at peak load and displacement. The h_c value is evaluated from the intercept of the initial unloading slope with the displacement axis, and the maximum displacement reached by the indenter [21]. The procedure used for the determination of the true zero of indentation depth conforms to the criteria adopted in Ref. [4].

3. Results and discussion

3.1. Development of crystallinity on annealing

Fig. 1 shows the WAXS patterns of the starting glassy PET and of the PET samples subsequently annealed at different temperatures, T_a. One can clearly observe the progressive development of crystallinity with increasing T_a. The sharp diffraction doublets observed at $2\theta=31.10$, 31.17 and 36.08, 36.17° are associated to the aluminum sample holder.

Fig. 2 shows the occurrence of crystallinity (α_{WAXS}) at $T_a \geq 120$ °C (Table 1). Open symbols are taken from Ref. [10] and relate to preceding microindentation studies in glassy PET samples annealed for 1–2 h. These data are included to recall the reader the usual stepwise increase of crystallinity upon crystallization. The dashed line in Fig. 2 is a guide to the eyes.

3.2. Influence of annealing temperature on the micromechanical properties

Fig. 3 shows the H and E variation with T_a (Table 1). Data taken from preceding microindentation studies of glassy annealed samples are also included [10]. The dashed lines are guides to the eyes. The conspicuous H and E increase at 120 °C could be immediately correlated to the development of crystallinity (Fig. 2). Moreover, the general E and H tendency to increase with increasing T_a above 120 °C, can also be correlated, at first sight, to the observed α_{WAXS} behaviour in the same temperature interval (Fig. 2). Fig. 4 (top) shows the increasing tendency of H and E to increase with the degree of crystallinity (both α_{WAXS} and α_{DSC} values have been included). It is now widely accepted that H of a semicrystalline material results

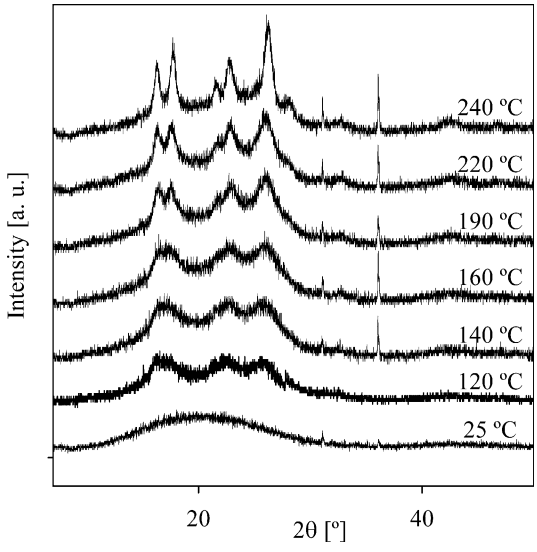

Fig. 1. WAXS patterns of the PET samples annealed at different temperatures, T_a. The sharp diffraction doublets near $2\theta=31$ and 36° are associated to the aluminum sample holder.

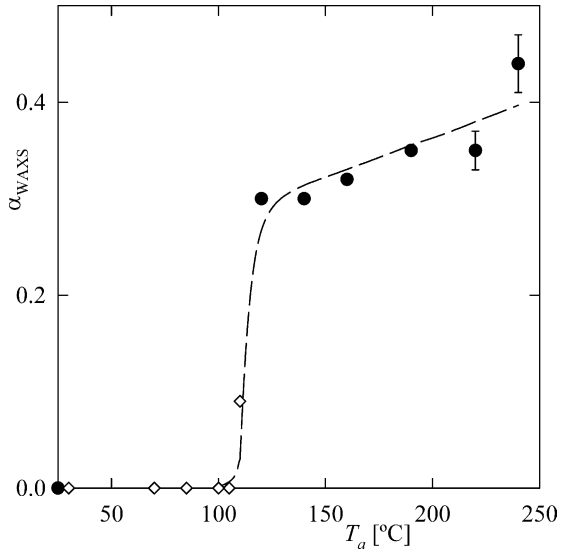

Fig. 2. Degree of crystallinity, as determined from WAXS, as a function of annealing temperature (solid symbols). For samples annealed below 220 °C, the error bars lie within the symbol size (open symbols are taken from Ref. [10]). The dashed line is a guide to the eyes.

from the contribution of the hardness of the crystalline and amorphous regions, H_c and H_a, respectively, following [1,6]:

$$H = H_c\alpha + H_a(1-\alpha) \quad (3)$$

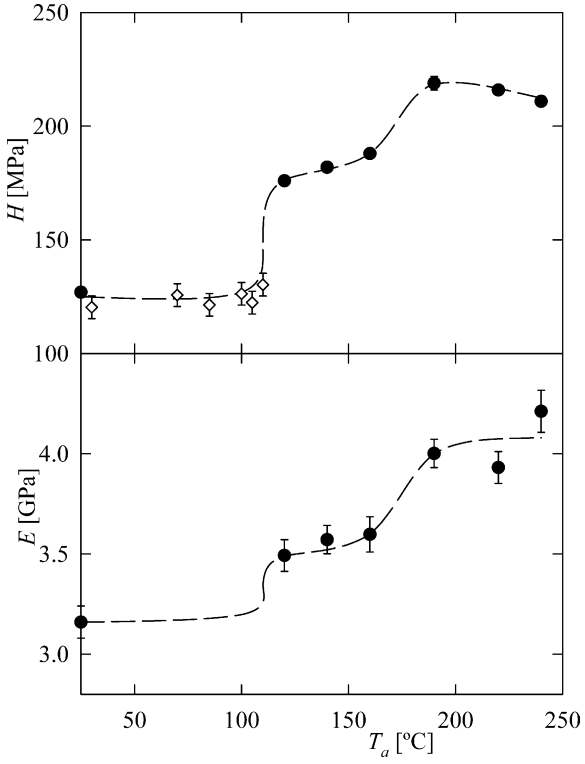

Fig. 3. Microhardness and elastic modulus values (top and bottom figures, respectively) as a function of annealing temperature (solid symbols). Error bars for the H data lie within the symbol size (open symbols are taken from Ref. [10]). The dashed lines are guides to the eyes.

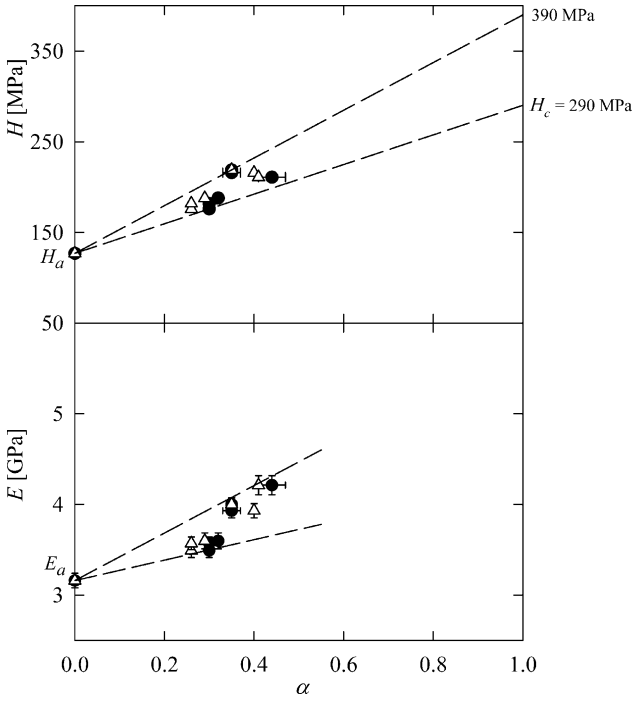

Fig. 4. H and E values (top and bottom figures, respectively) versus degree of crystallinity. Solid symbols: α_{WAXS}; open symbols: α_{DSC} (error bars for the H data and most of those associated to the α data lie within the symbol size).

Hence, assuming $H_a = 127$ MPa (hardness value measured for the amorphous material), then, one can calculate the H_c value for each of the annealed samples. The area enclosed between the dashed straight lines in Fig. 4 (top) intercepts the right-hand y-axis giving rise to the range of H_c values for the annealed PET series ($H_c = 290$–390 MPa). Fig. 4 (bottom) suggests that a parallel E increase with increasing α is observed. A number of models have been proposed to account for the E variation with α [23]. However, a limited number of papers have provided experimental evidence of the influence of α on the elastic properties of polymer materials, measured by means of indentation measurements [24,25]. The present results support a variation of the E values with α similar to that of hardness ($E/H \approx 20$, see Table 1). In addition, the E/H ratio found is in agreement with previously reported data [25].

The results of Fig. 4 suggest that not only crystallinity monitors the mechanical properties of the annealed materials. The fact that different H_c values are obtained for the various annealed materials indicates that other structural features than crystallinity influence the extent of the crystal reinforcement. A detailed discussion on this issue is offered below.

3.3. Nanostructural changes on annealing

Fig. 5 shows the variation of the crystal thickness, l_c, with annealing temperature (Table 1). The interface distribution function for the samples annealed at 120, 140 and 160 °C was

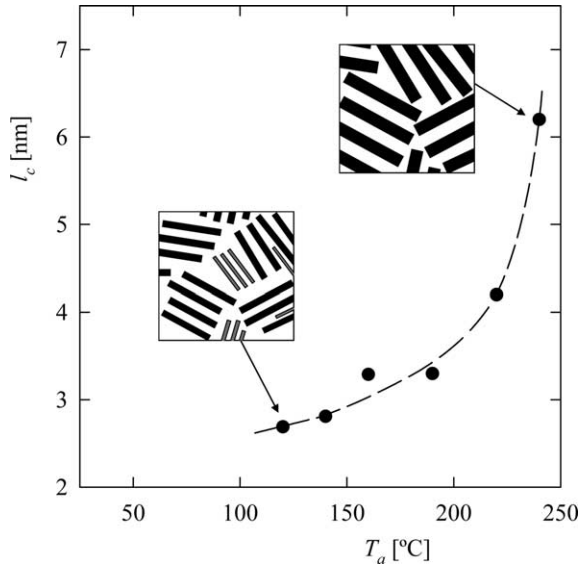

Fig. 5. Crystal thickness, as determined from the analysis of the SAXS data by means of the IDF, as a function of annealing temperature.

best fitted to a model comprising two different lamellae stacks (Fig. 5). However, the accuracy of the structural parameters derived was limited due to the difficulty in separating both components, especially for the sample annealed at 140 °C. Due to this limitation, the data shown in Fig. 5 (Table 1) for $T_a \leq 160$ °C correspond to the fitting of the IDFs to a model of single lamellae stacks. On the other hand, the IDF functions of the samples annealed at $T_a \geq 190$ °C were best fitted to a model of lamellar stacks with a unimodal thickness distribution. These results are in consonance with the heating DSC runs of the annealed PET samples, where two melting peaks are observed for the low temperature annealed samples: The melting peak at low temperatures seems to be associated to secondary crystallization while the high temperature peak could be related to the primary process. In contrast, a single endothermic peak, associated to primary lamellar stacks, is observed for samples annealed above 190 °C. Fig. 5 schematically shows the nanostructural model associated to the low and the high temperature annealed material. In the low temperature model, the possibility of lamellae insertions during secondary crystallization, in addition to the development of new lamellae stacks, is indicated. The fact that the linear degree of crystallinity, α_L ($\alpha_L = l_c/(l_c + l_a)$), is only slightly larger than the volume degree of crystallinity (Table 1) could favor the occurrence of lamellae insertion.

3.4. The influence of the b-parameter on the microhardness values

Fig. 5 shows an apparent l_c increase with increasing T_a, especially at 240 °C. It is now well established that the crystal thickness influences the H_c values following [1]:

$$H_c = \frac{H_c^{\infty}}{1 + (b/l_c)} \quad (4)$$

Here, H_c^{∞} is the hardness of an infinitely thick crystal ($H_c^{\infty} = 418$ MPa for PET [11]). The b-parameter is related to the ratio between the surface free energy of the crystals, σ_e, and the energy required to plastically deform them through a number of shearing planes, Δh ($b = 2\sigma_e/\Delta h$). In the preceding section, we have seen that the range of H_c values for the annealed PET series lies in the range $H_c = 290$–390 MPa (Fig. 4). At this point, one may enquire whether the distribution of H_c values is related to variations in the material lamellar thickness. In this case, the $1/H_c$ values should vary linearly with $1/l_c$ (Eq. (4)), the slope being b/H_c^{∞} and the y-axis intercept $1/H_c^{\infty}$.

Fig. 6 shows the variation of the $1/H_c$ data as a function of $1/l_c$. Assuming $H_c^{\infty} = 418$ MPa [11], significant deviations of the data to a linear fit are found. This finding suggests that the b-parameter does not remain constant for all the annealed samples. Fig. 7 shows, indeed, the plot of b versus T_a. The b-value for each annealed material is calculated using Eq. (4) ($H_c^{\infty} = 418$ MPa, l_c is taken from Fig. 5 and H_c is calculated using Eq. (3) with $H_a =$ 127 MPa). From these data, one can see that the b-value at 190 °C is slightly smaller, and that at 240 °C larger to some extent, with respect to the average b-value for the other materials ($b \approx 0.8$ nm). This would explain why the microhardness values tend to decrease within the range 190 °C $\leq T_a \leq$ 240 °C (Fig. 3), despite the crystal thickness values conspicuously increase in this temperature range (Fig. 5). The question now is whether the variation of the b parameter for high annealing temperatures (Fig. 7) can be independently attributed to changes in the material properties. As mentioned above, the b-parameter is related to the surface free energy of the crystals and to the energy required for plastic deformation of the crystal blocks, ($b = 2\sigma_e/\Delta h$). To explore the possibility of the σ_e values accounting for the

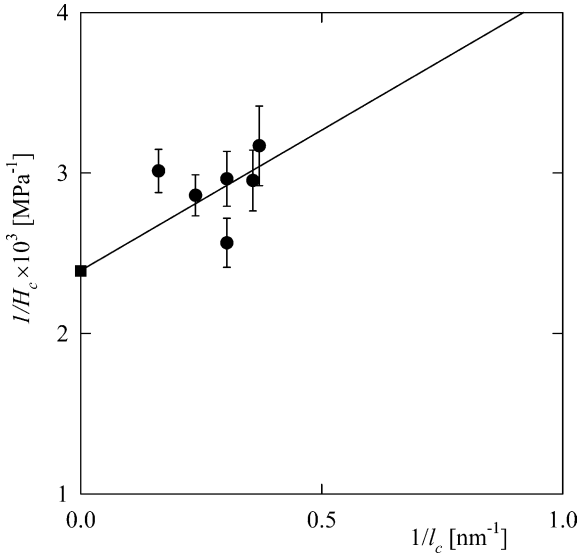

Fig. 6. $1/H_c$ values versus l_c. The square symbol represents $1/H_c^{\infty}$ ($H_c^{\infty} = 418$ MPa [11]).

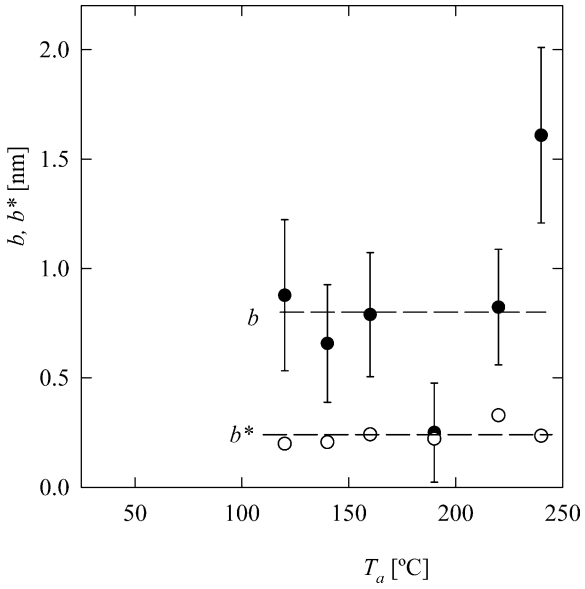

Fig. 7. The b-mechanical and b^*-thermodynamical values as a function of T_a.

b dependence observed with T_a, we have independently evaluated the σ_e values for each annealed sample, using Gibbs–Thomson equation:

$$T_m = T_m^\infty \left(1 - \frac{b^*}{l_c}\right) \quad (5)$$

where T_m^∞ is the equilibrium melting point ($T_m^\infty = 558$ K [11]), and $b^* = 2\sigma_e/\Delta h_f$, Δh_f being the melting enthalpy. Fig. 7 also includes the b^* values for the annealed PET samples, calculated from Eq. (5), using $T_m^\infty = 558$ K, and the T_m and l_c values taken from Table 1 and Fig. 5, respectively. For samples with two melting endotherms, we have used the high melting peak for the derivation of b^*; the minor population of secondary lamellae has been neglected as a first approximation. One can see that there is no significant variation of b^* with T_a, hence, the σ_e values should remain constant throughout the annealed series. Consequently, the changes of the b-parameter observed in Fig. 7 should be attributed to the Δh parameter.

3.5. The enthalpy required for plastic deformation of the crystals: Connectivity via the amorphous phase

In view of the preceding analysis, the significant hardness enhancement observed at $T_a = 190$ °C, followed by a slight H decrease (Fig. 3), despite the degree of crystallinity (Fig. 2) and, more distinctly, the crystal thickness (Fig. 5) values increase within the range 190 °C $\leq T_a \leq$ 240 °C, could be explained as follows:

1. For $T_a = 190$ °C, lamellar stacks with a unimodal thickness distribution are distinguished from the SAXS IDF analysis, although a small melting endotherm is observed at low temperatures by means of DSC. The SAXS analysis of the samples crystallized at $T_a < 190$ °C suggest that two types of lamellae stacks coexist in these materials, in agreement with a well differentiated low melting endotherm in the DSC scan. On the other hand, samples annealed at $T_a > 190$ °C clearly display one DSC endothermic peak and also a single population of lamellae stacks as revealed by SAXS. Hence, the sample annealed at 190 °C exhibits a nanostructure in the border line between the two types of crystallization processes, at high and low T_a, depicted schematically in Fig. 5. In addition, it is noteworthy that the amount of amorphous material outside the lamellae stacks, $\phi_a = 1 - (\alpha_{WAXS}/\alpha_L)$, is considerably reduced by annealing at 190 °C to 15%, with respect to that for lower annealing temperatures ($\phi_a = 23 - 32\%$ for $T_a = 120$–160 °C), approaching the ϕ_a values at 220 °C (17%) and 240 °C (6%). Hence, one may speculate that the significant H enhancement observed at 190 °C could be associated to a more efficient reinforcement of the material due to a homogeneous dispersion of the 'hard component' (nanocrystals). Following this argument, the H increase at 190 °C could be envisaged in two different ways, however, the results presented in this paper cannot discern which one of the following effects prevail: (i) Either the energy required for plastic deformation of the crystals Δh is larger at 190 °C (consequently the b-parameter is lower, and hence, H_c increases) than that at $T_a < 190$ °C, due to a more homogeneous distribution of the lamellae which would enhance the connectivity between neighbouring crystals; (ii) or the average hardness value of the amorphous material increases at 190 °C with respect to that at lower T_a due to the fact that the amount of amorphous material outside the lamellar stacks is substantially reduced. The hardness of the amorphous layers constrained between the crystalline regions could be larger than that of the amorphous regions between lamellae stacks (role of the rigid amorphous phase). In this case, assuming $b = 0.8$ nm, we can estimate an average value for the hardness of the amorphous regions, to be of $H_a = 150$ MPa.
2. For 190 °C $< T_a \leq$ 240 °C, the hardness tendency to decrease with increasing annealing temperature could be associated to a sample degradation process, expected to occur at high temperatures. Chain scission could take place, leading to a decrease in the sample molecular weight. Dynamic mechanical thermal analysis studies in course, to be published in a separate study [26], suggest that the glass transition temperature shifts towards lower values for the sample annealed at 220 °C, with respect to the one treated at 190 °C. These findings are in support of a chain scission process occurring at high temperatures, which could result in: (i) A reduction in the number of entanglements within the amorphous regions between crystals, and (ii) a decrease of the number of tie molecules connecting adjacent crystals; both effects

would facilitate the material deformation upon an external compressive stress, in agreement with the *b*-increase (Δh decrease) discussed in the preceding section. In addition, chain-scission could also result in a softening of the amorphous regions as a consequence of a lower sample molecular weight. Hence, the extent of the *b*-increase shown in Fig. 7 for $T_a = 240$ °C could be modulated by a H_a decrease with respect to the H_a values measured at lower annealing temperatures.

In conclusion, the present results suggest that the distribution of the nanocrystal stacks within the amorphous matrix could modulate the extent of the reinforcing effect of the former hard component on the softer phase. In particular, the connectivity between neighbouring crystals (number of taut and tie molecules) should play an important role in the mechanical response of PET to indentation. In addition, the constrained amorphous regions between adjacent crystal lamellae could exhibit improved mechanical properties, in contrast to those of the thicker amorphous layers between stacks.

Acknowledgements

The authors acknowledge the Ministerio de Educación y Ciencia (Grant No FIS2004-01331), Spain, for the generous support of this investigation. This work was supported by the European Community—Research Infrastructure Action under the FP6 'Structuring the European Research Area' Programme (through the Integrated Infrastructure Initiative 'Integrating Activity on Synchrotron and Free Electron Laser Science': Project II-04-029 EC). The authors thank Dr Gennaro Gentile, ICTP, CNR, Naples, for the determination of the molecular weight of the PET investigated.

References

[1] Baltá Calleja FJ, Fakirov S. Microhardness of polymers. Cambridge, UK: Cambridge University Press; 2000.
[2] Seidler S, Koch T. J Macromol Sci, Phys 2002;B41(4–6):851.
[3] Ashcroft IA, Spinks GM. J Mater Res 1996;11(2):529.
[4] Briscoe BJ, Sebastian KS, Sinha SK. Philos Mag 1996;A74(5):1159.
[5] Baltá Calleja FJ, Fakirov S. Trends Polym Sci 1997;5(8):246.
[6] Beake BD, Leggett GJ. Polymer 2002;43:319.
[7] Minkova L, Yordanov H, Zamfirova G, Magagnini PL. Colloid Polym Sci 2002;280:358.
[8] Flores A, Baltá Calleja FJ, Attenburrow GE, Bassett DC. Polymer 2000;41:5431.
[9] Hochstetter G, Jimenez A, Loubet JL. J Macromol Sci Phys 1999; B38(5–6):681.
[10] Santa Cruz C, Baltá Calleja FJ, Zachmann HG, Stribeck N, Asano T. J Polym Sci, Part B: Polym Phys 1991;29:819.
[11] Baltá Calleja FJ, Öhm O, Bayer RK. Polymer 1994;35(22):4775.
[12] Puente Orench I, Ania F, Baer E, Hiltner A, Bernal T, Baltá Calleja FJ. Philos Mag 2004;84(18):1841.
[13] Xia Z, Sue HJ, Wang Z, Avila-Orta CA, Hsiao BS. J Macromol Sci Phys 2001;B40(5):625.
[14] Haubruge HG, Jonas AM, Legras R. Macromolecules 2004;37:126.
[15] Wünderlich B. Prog Polym Sci 2003;28:383.
[16] Lin J, Shenogin S, Nazarenko S. Polymer 2002;43:4733.
[17] Bartolotta A, Di Marco G, Farsaci F, Lanza M, Pieruccini M. Polymer 2003;44:5771.
[18] Asano T, Baltá Calleja FJ, Flores A, Tanigaki M, Mina MF, Sawatari C, et al. Polymer 1999;40:6475.
[19] Kong Y, Hay JN. Polymer 2003;44:623.
[20] Flores A, Pietkiewicz D, Stribeck N, Roslaniec Z, Baltá Calleja FJ. Macromolecules 2001;34(23):8094.
[21] Oliver WC, Pharr GM. J Mater Res 1992;7(6):1564.
[22] Birley AW, Haworth B, Batchelor J. Physics of plastics. New York: Oxford University Press; 1991.
[23] Peterlin A. Macromol Chem 1973;8:277.
[24] Flores A, Baltá Calleja FJ, Asano T. J Appl Phys 2001;90(12):6006.
[25] Krumova M, Flores A, Baltá Calleja FJ, Fakirov S. Colloid Polym Sci 2002;280:591.
[26] Pieruccini M, Di Marco G. Unpublished results.